

Available online at www.sciencedirect.com

SciVerse ScienceDirect

Scripta Materialia 68 (2013) 158-161



www.elsevier.com/locate/scriptamat

Influence of the thermal route on the peak-aged microstructures in an Al-Mg-Si aluminum alloy

S. Pogatscher,^{a,*} H. Antrekowitsch,^a H. Leitner,^b A.S. Sologubenko^c and P.J. Uggowitzer^d

^aInstitute of Nonferrous Metallurgy, Montanuniversitaet Leoben, Franz-Josef-Strasse 18, 8700 Leoben, Austria
^bDepartment of Physical Metallurgy and Materials Testing, Montanuniversitaet Leoben, Franz-Josef-Strasse 18, 8700 Leoben, Austria
^cLaboratory for Nanometallurgy, Department of Materials, ETH Zurich, Wolfgang-Pauli-Strasse 10, 8093 Zurich, Switzerland
^dLaboratory of Metal Physics and Technology, Department of Materials, ETH Zurich, Wolfgang-Pauli-Strasse 10, 8093 Zurich, Switzerland

Received 10 July 2012; revised 5 October 2012; accepted 8 October 2012 Available online 13 October 2012

The influence of the thermal route on the peak-aged microstructures in an Al–Mg–Si aluminum alloy was investigated by atom probe tomography and transmission electron microscopy. Direct artificial aging induced a monomodal size distribution of β'' -precipitates, while for artificial aging after natural pre-aging a bimodal size distribution was found. This difference can be explained by the impact of lattice defects on the β'' -nucleation. β'' is supposed to contain Al and exhibits a high Mg/Si ratio in the studied alloy.

© 2012 Acta Materialia Inc. Published by Elsevier Ltd. All rights reserved.

Keywords: Aluminum alloys; Aging; Precipitation; Vacancies; Phase transformation kinetics

For the well-known aluminum alloy AA6061 a strong adverse influence of natural pre-aging on kinetics and T6 strength has been reported [1-4]. This phenomenon, occurring in the rich Al-Mg-Si alloys, is commonly called the "negative effect" and has been linked to a coarser distribution of precipitates than that formed by direct artificial aging [4,5]. The simplified precipitation sequence of AA6061 [6] can be described as super-saturated solid solution (SSSS) → clustering stage → Mg, Si co-clusters \rightarrow Guiner-Preston (GP)-I zones, pre- $\beta'' \rightarrow \beta'' \rightarrow B'$, $\beta' \to \beta\text{-Mg}_2\text{Si}.$ Various other precipitates [7] have also been reported. The early stages of aging resulting in the formation of Mg, Si co-clusters [8] take place in several individual steps that have not yet been clearly distinguished [9]. Atom probe tomography (APT) is currently the only technique for visualizing such small clusters [10], but even this method is operating at its limit for this purpose. The earliest precipitates in the sequence which produce a distinct contrast for transmission electron microscopy (TEM) identification are GP-I zones [11]. These are thermally more stable

clusters, contain more solute atoms and are spherical, with a typical size of 1–3 nm [8,11–13]. Note that the needle-like pre-β" phase [14] has been described as the most developed GP-I zone. Spherical particles, often termed GP-I zones [4,8,11,12,15], might be earlier stages of preβ". However, this is in accordance with the fact that GP-I zones have been reported to transform to β'' [16]. β'' needles [13,17] are the typical precipitates under T6 conditions in AA6061 [6]. They have a base-centered monoclinic structure and are aligned along $\langle 100 \rangle_{Al}$, being fully coherent only along the needle-axis. Although the chemical composition of the β'' phase has been proposed as Mg₅Si₆ [13,17], it has become clearer in the past few years that the exact composition of β'' seems to be strongly influenced by the composition of the alloy [12,18,19] and has to be clarified for each individual alloy. Note that the precursor of β'' (pre- β'') exhibits a similar structure only with slightly different lattice parameters [7,14] resulting in very similar TEM images and diffraction patterns [16]. For over-aged conditions, the rod-shaped phases β' [20], B' [21], and a large number of other lath- or rodshaped phases, have been reported [7].

The studied alloy AA6061 (Mg 0.92, Si 0.58, Cu 0.09, Fe 0.25, Cr 0.08, Mn 0.05, Zn 0.03 and Ti 0.05, at.%) was provided by AMAG Rolling in the form of wrought

^{*} Corresponding author. Tel.: +43 6644256275; fax: +43 38424025202; e-mail: stefan.pogatscher@unileoben.ac.at

plate. Solution heat treatment was conducted in a circulating air furnace at 570 °C for 1.2 ks. Direct artificial aging and artificial aging after long-term natural preaging of 1.2×10^6 s after quenching was performed at $170 \,^{\circ}\text{C}$ for $2.88 \times 10^4 \,\text{s}$. Needle-shaped specimens for APT were prepared via a standard two-step method [22]. APT was performed on a LEAP™ 3000 X HR atom probe at a temperature of -238 °C with a pulse of 15% under ultra-high fraction vacuum (<10⁻¹⁰ mbar). The reconstruction procedure and analysis were conducted using the software package IVAS 3.6.0[™] from CAMECA. TEM specimens were prepared by the standard route of grinding, dimpling and finally electrolytic polishing as described in Ref. [6]. Conventional TEM (CTEM), high-resolution TEM (HRTEM) and scanning TEM (STEM) studies were performed on an FEI Tecnai F30 machine operated at 300 kV.

Figure 1 shows three-dimensional (3-D) reconstructions of the atom positions for Mg. Si and Cu. and isoconcentration surfaces of Mg embedded in the Al matrix with corresponding proximity histograms for Al, Mg, Si and Cu based on short needles and long needles for the two T6 microstructure variants. To visualize the precipitation microstructure more clearly, isoconcentration surfaces, with an arbitrary threshold value of 2.8 at.% Mg, which is three times higher than the average Mg concentration of the alloy, were used. The individual precipitates were distinguished according to their morphology and composition. Direct artificial aging (Fig. 1a) revealed a dense monomodal distribution of short needles oriented in three directions perpendicular to each other with a high number density $(2.9 \times 10^{23} \text{ m}^{-3})$. In addition, smaller isosurfaces, which might include GP-I zones and a few co-clusters [4], are present. Artificial aging after long-term natural preaging (Fig. 1b) revealed two morphologies of needles oriented in three perpendicular directions. In addition

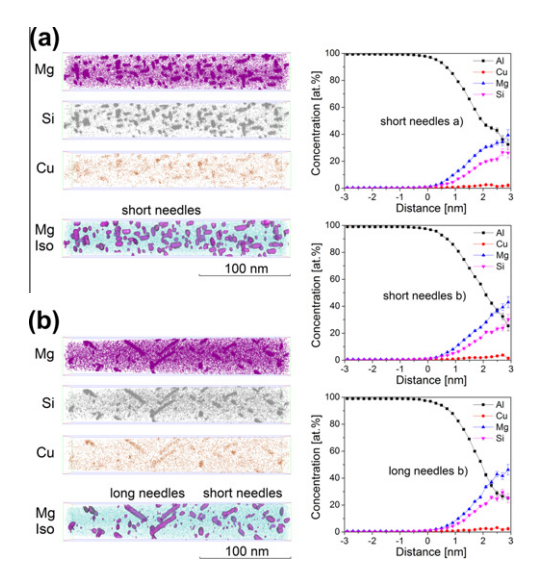


Figure 1. Three-dimensional (3-D) reconstructions of the atom positions for Mg, Si and Cu and isoconcentration surfaces of Mg embedded in the Al matrix with corresponding proximity histograms for Al, Mg, Si and Cu based on short needles and long needles for (a) direct artificial aging and (b) artificial aging after long-term natural pre-aging (all in T6 condition).

to short needles $(0.8 \times 10^{23} \,\mathrm{m}^{-3})$, long needles with a much higher aspect ratio were found in a low number density ($\sim 0.1 \times 10^{23} \,\mathrm{m}^{-3}$). Moreover, smaller and nearly spherical isosurfaces, very likely indicating coclusters, and a few GP-I zones are present [4]. Proxigrams [23,24] based on the isosurfaces shown in Figure 1 were used to compare the chemical composition of various needle-like precipitates. The core composition of short needles observed after direct artificial aging was found to be 34 ± 3.3 at.% Al, 3.3 ± 1.8 at.% Cu, 37 ± 3.4 at.% Mg and 26 ± 3.0 at.% Si. Short needles induced by artificial aging after long-term natural preaging revealed 29 ± 3.0 at.% Al, 2.6 ± 1.0 at.% Cu, 41 ± 3.3 at.% Mg and 27 ± 3.0 at.% Si. The long needles exhibited a composition of 26 ± 3.0 at.% 2.0 ± 0.9 at.% Cu, 44 ± 3.1 at.% Mg and 27 ± 2.8 at.% Si in the core. A comparison of the proximity histograms revealed no distinct discrepancy for the individual needles studied. The average solute concentration seems to be slightly higher in the short and long needles generated by artificial aging after long-term natural pre-aging than that observed in the short needles produced by direct artificial aging, but the differences are not significant. A cluster search algorithm based on the maximum separation method, taking into account Mg, Si and Cu as involved solutes, was also utilized [25]. The separation distance (d_{max}), surround distance (L) and erosion distance (dero) were determined based on the method described in Ref. [26] and were set to 0.48. Note the numbers of atoms discussed are all detected values and do not take the detection efficiency (36%) into account. The results of the cluster search algorithm are given in Table 1.

Because the cluster search includes the shell of the studied precipitates it revealed a higher Al content compared to the core composition deduced from the proxigrams. However, it showed no significant differences between the needles occurring during the two thermal histories. Note that the average number of solutes in the long needles is much higher than in the short needles. Numerous previous studies have described needles occurring in peak-aged conditions in AA6061 as β" [6,11]. Obviously the Mg/Si ratio of all observed needles is higher than for β" precipitates with Mg₅Si₆ stoichiometry [13,17]. Nevertheless, our results are consistent with other APT studies on AA6061 [12] and balanced Al-Mg₂Si alloys [8,27], which reported even higher Mg/Si ratios for β'' . In addition, a significant Al content in the needles investigated was observed. This is consistent with the findings of Hasting et al. [18], who claimed that Mg₅Al₂Si₄ [19] may be energetically more beneficial than

Table 1. Results of the cluster search algorithm.

	Direct artificial aging	Artificial aging after natural pre-aging	
	Short needles	Short needles	Long needles
Solutes	500 ± 200	700 ± 300	2700 ± 600
Al (at.%)	45 ± 5.1	44 ± 4.9	43 ± 4.0
Cu (at.%)	2.4 ± 0.9	2.8 ± 0.8	2.3 ± 0.7
Mg (at.%)	32 ± 3.3	32 ± 2.9	33 ± 3.2
Si (at.%)	20 ± 2.4	21 ± 2.3	21 ± 1.9
Mg/Si	1.6 ± 0.2	1.5 ± 0.2	1.6 ± 0.2

Download English Version:

https://daneshyari.com/en/article/1499193

Download Persian Version:

https://daneshyari.com/article/1499193

Daneshyari.com